Validation of ERBS Scanner Radiances

RICHARD N. GREEN AND LEE M. AVIS

Atmospheric Sciences Division, NASA/Langley Research Center, Hampton, Virginia

(Manuscript received 6 February 1995, in final form 27 November 1995)

ABSTRACT

The earth radiation budget satellite (ERBS) has made broadband scanner measurements of the earth radiance for over 5 years. The redundancy between the shortwave, longwave, and total scanning radiometers and data averages have been used to validate the long-term consistency among the measurements and to establish how measurement drift has affected the archived top-of-the-atmosphere fluxes. The total channel gain at night was found to be unchanged over a 4-yr test period. Relative to the total channel at night, the longwave channel sensitivity decreased by 0.5% over the same 4 years and the shortwave channel was unchanged. The shortwave part of the total channel, however, gradually increased in gain by 1.3%. Only the daytime longwave flux was affected by these changes. It drifted upward depending on the scene shortwave component. Over 4 years, the clear ocean daytime longwave flux increased by 0.2% and overcast scenes by 2.6%. For all scenes in the Tropics, the daytime longwave flux increased by less than 1% in 4 years. There was no statistical evidence that the daytime shortwave or nighttime longwave fluxes had drifted.

1. Introduction

The Earth Radiation Budget Experiment (ERBE) is a three-satellite system to measure the radiation budget at the top of the atmosphere (TOA). Each satellite carries both narrow-angle scanning radiometers and wide-angle nonscanning radiometers. Two of the satellites, *NOAA-9* and *NOAA-10,* are in polar sun-synchronous orbit. The earth radiation budget satellite (ERBS) is the third satellite and is in a precessing orbit relative to the sun with an inclination of 57°. The details of the science objectives and implementation of the ERBE are given by Barkstrom (1984) and Barkstrom and Smith (1986). This paper examines the long-term stability of the ERBS scanning radiometers and thus the stability of the archived ERBE products (Barkstrom et al. 1990).

The ERBE scanning radiometers are cross-track scanners with spatial resolution of about 30 km × 45 km at nadir. The three scanning channels consist of a total channel (TOT), which measures all radiation from 0.2 to more than 50 μm, a shortwave channel (SW) with a range of 0.2–5 μm, and a longwave channel (LW) with a range from 5 to 50 μm. Kopia (1986) gives a complete discussion of the ERBE scanner radiometers. Lee et al. (1989) gives the conversion of the radiometer measurements from counts to filtered radiances.

Corresponding author address: Richard N. Green, Langley Research Center, NASA/Atmosp. Science Div., Code 420, Hampton, VA 23681-0001.

Since early spacecraft radiometers exhibited degradation of their response with time (Bandeen et al. 1965; Bandeen 1982; House et al. 1986), the ERBE design included a complete onboard calibration system (Barkstrom 1984) to monitor instrument drift. The SW and TOT channels viewed the Mirror Attenuator Mosaic (MAM), which is a solar diffuser plate. The SW channel also viewed the Shortwave Internal Calibration System (SWICS), which consists of a tungsten lamp monitored by a silicon photodiode. And finally, the LW and TOT channels viewed internal blackbodies.

Solar calibration checks for the SW and TOT channels using the MAM were conducted on ERBS every two weeks from November 1984 through October 1985. The results from the MAM data are given by Lee et al. (1992) and indicate that the gain on the SW channel was constant to ±2%. On 28 February 1985, the ERBS scanners accidentally viewed the sun directly and caused a 6.5% decrease in the gain of the shortwave part of the TOT channel (Weaver et al. 1991; Lee et al. 1992). This dramatic change was shown by the MAM results and by several other validation parameters and was corrected by adjusting the spectral correction coefficients as discussed later. The MAM in-flight calibration results are limited in that we only have MAM data for the first of the 5 years of ERBS scanner data. This short calibration period and noise in the MAM data ensures only that the gains did not change by more than 2% within the first year. It gives no information on the last 4 years of data or on shortwave offset drift.

The calibration of the SW channel was monitored in-flight over the 5-yr data period by viewing the

SWICS every 2 weeks. The results given by Lee et al. (1993) show that the shortwave scanner response was constant to ±1%. However, the response of the silicon photodiode system used to evaluate the stability of the tungsten lamps was found to degrade by as much as 6% during the first 2 years in orbit. Since the stability of the SWICS could not be established, the data were interpreted to mean that both the SWICS and the SW channel were stable over the 5 years to within ±1%. It would be unlikely that one would drift and the other would drift in the opposite direction to produce the constant results. As with the MAM, the SWICS used a differencing technique of lamp-on and lamp-off so that no information is given on the SW channel offsets. Also, there is no information on the shortwave part of the TOT channel.

Internal blackbodies were used in-flight to monitor the radiometric gains of the LW channel and the longwave part of the TOT channel. The time series of blackbody measurements indicate that the gains were stable to better than 1% over the 5-yr period (Lee and Barkstrom 1991). The basic measurement is the difference in the radiometer's output signals corresponding to observations of the blackbodies and cold space. Here again, there is no information of longwave offset drift.

Because of the limitations of the onboard calibration system to detect changes less than 1% in gain and the absence of any offset detection, an independent study of the long-term stability of the ERBS scanners has been conducted by making use of the three channel redundancy and long-term data averages. Only the earth-viewing radiances have been used. First, we compare the LW and TOT channels at night. Because of its flat spectral response and stability, the longwave part of the TOT channel was taken as the reference and the other two channels compared to it. The LW channel was matched to the TOT channel at night with new spectral correction coefficients and used to transfer the reference level from night to day. The daytime longwave was then determined from the TOT channel minus the SW channel and compared to the adjusted LW channel. In this way, the stability of the SW channel and the shortwave part of the TOT channels were inferred.

2. Top-of-the-atmosphere flux

Determination of the TOA fluxes as archived on the ERBE S8 data product involves use of 12 ERBE scene types, the spectral correction algorithm, and the inversion process (Smith et al. 1986). Both the spectral correction algorithm and the inversion process are a function of the scene that is viewed. The ERBE scene types consist of four surface types (ocean, land, snow, desert) and one mixed surface type of land and ocean (coastal). These five surface types are combined with four cloud conditions (clear, partly cloudy, mostly cloudy, overcast) to define the 12 ERBE scene types as given in Table 1. The ERBE data processing first identifies the instantaneous scene type from the ERBE scanner data with a maximum-likelihood estimation algorithm (Wielicki and Green 1989). The measured filtered radiances are then unfiltered with the spectral correction coefficients (section 3) for the identified scene and inverted to flux at the TOA by

$$\hat{F}^j = \frac{\pi I^j}{R_i(\Omega)}, \tag{1}$$

where I^j (j = SW, LW) are the ERBE unfiltered radiances, $\hat{F}^j$ are the corresponding flux estimates at the TOA, and $R_i(\Omega)$ are the angular distribution models (ADM) that relate radiance to flux (Suttles et al. 1988, 1989). The viewing geometry is represented by Ω, and the index i denotes different scene types. The longwave radiance ADMs (limb-darkening models) are a function of viewing zenith, while the shortwave radiance ADMs (bidirectional models) are a function of three angles: viewing zenith, solar zenith, and relative azimuth. Thus, the inversion of radiances to fluxes at the TOA involves determining the scene type (i), evaluating $R_i(\Omega)$, and applying (1). The purpose of this paper is to examine the long-term change in the TOA flux due only to drift in the scanner measurements. The errors in TOA flux from spectral correction errors, scene misidentification, and ADM errors do not change with time. Examination of these error sources is outside the purpose of this paper.

3. Spectral correction

The spectral correction algorithm corrects the radiometric measurements for the imperfect spectral response of the optical path in the instrument. Radiation from the scene is collected and focused by primary and secondary mirrors. The radiation passes through the spectral filter (for the SW and LW channels), impinges on the detector, and causes a signal that is sampled and processed by the electronics, resulting in a filtered measurement. To correct this filtered signal, we need to

TABLE 1. ERBE scene types.

Index	Scene types
1	Clear ocean
2	Clear land
3	Clear snow
4	Clear desert
5	Clear land–ocean mix (coastal)
6	Partly cloudy over ocean
7	Partly cloudy over land or desert
8	Partly cloudy over land–ocean mix
9	Mostly cloudy over ocean
10	Mostly cloudy over land or desert
11	Mostly cloudy over land–ocean mix
12	Overcast

know the spectral response of the individual channels and the spectral nature of the observed scene. The objective is to determine the reflected (or shortwave) radiation below 5 μm and the emitted (or longwave) radiation above 5 μm.

We model the "filtered" scanner measurements as

$$m_f^j = \int_0^\infty S_\lambda^j I_\lambda d\lambda + \epsilon^j \quad j = \text{SW, TOT, LW,} \quad (2)$$

where λ (μm) is wavelength; I_λ (W m^{-2} sr^{-1} μm^{-1}) is the spectral radiance incident on the instrument; S_λ is the normalized spectral response of the instrument (Fig. 1) such that $0 \leq S_\lambda \leq 1$; ϵ (W m^{-2} sr^{-1}) is the instrument error with mean 0 and variance σ_ϵ^2, which results from count conversion error, instrument noise, and any instrument error except spectral dependance effects; and j denotes the shortwave, total, or longwave scanner channel. We desire to estimate the "unfiltered" scanner measurements, which are defined as

$$m^i = \int_0^\infty C_\lambda^i I_\lambda d\lambda \quad i = \text{SW, LW,} \quad (3)$$

where C_λ^i is the ideal instrument response, or

$$C_\lambda^{\text{SW}} = \begin{cases} 1, & 0 \leq \lambda < 5\ \mu\text{m} \\ 0, & \text{otherwise} \end{cases}$$

$$C_\lambda^{\text{LW}} = \begin{cases} 1, & 5 \leq \lambda \leq 200\ \mu\text{m} \\ 0, & \text{otherwise.} \end{cases}$$

Let us consider I_λ and ϵ as random variables so that both the filtered and unfiltered measurements are random variables. We desire to estimate the unfiltered measurements from the filtered measurements given the statistics of I_λ and ϵ. For simplicity, define the random vector of filtered measurements $\mathbf{Y}$ and the random vector of unfiltered measurements $\mathbf{X}$ as

$$\mathbf{Y} = \begin{bmatrix} m_f^{\text{SW}} \\ m_f^{\text{TOT}} \\ m_f^{\text{LW}} \end{bmatrix} \quad \mathbf{X} = \begin{bmatrix} m^{\text{SW}} \\ m^{\text{LW}} \end{bmatrix}.$$

We will assume a linear estimator $\hat{\mathbf{X}} = \mathbf{B}\mathbf{Y}$ and choose to minimize the diagonal terms of the matrix $E[(\hat{\mathbf{X}} - \mathbf{X})(\hat{\mathbf{X}} - \mathbf{X})^{\text{T}}]$ where $E[\mathbf{X}]$ is the statistical expectation operator. This estimator is called the minimum mean-square-error estimator. From the Gauss–Markoff theorem (Liebelt 1967), we have

$$\hat{\mathbf{X}} = E[\mathbf{X}\mathbf{Y}^{\text{T}}](E[\mathbf{Y}\mathbf{Y}^{\text{T}}])^{-1}\mathbf{Y}. \quad (4)$$

We will define the quantities $E[\mathbf{X}\mathbf{Y}^{\text{T}}]$ and $E[\mathbf{Y}\mathbf{Y}^{\text{T}}]$ empirically from data. The general elements are

$$E[\mathbf{X}^i\mathbf{Y}^j] = \int_0^\infty \int_0^\infty C_\lambda^i S_{\lambda'}^j E[I_\lambda I_{\lambda'}] d\lambda d\lambda' \equiv \overline{\mathbf{X}^i\mathbf{Y}^j}$$

$$i = \text{SW, LW,} \quad j = \text{SW, TOT, LW}$$

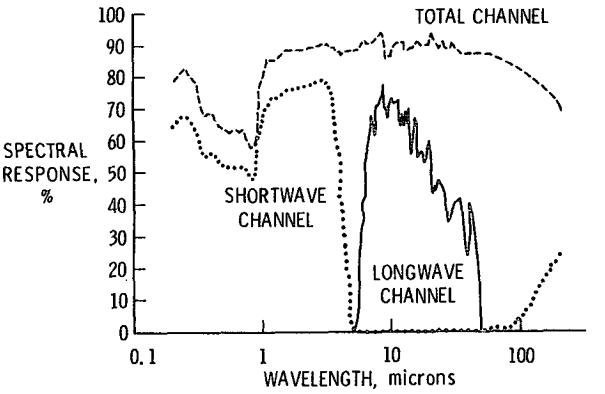

FIG. 1. Spectral response functions for ERBS scanning radiometers.

$$E[\mathbf{Y}^r\mathbf{Y}^s] = \int_0^\infty \int_0^\infty S_\lambda^r S_{\lambda'}^s E[I_\lambda I_{\lambda'}] d\lambda d\lambda' \equiv \overline{\mathbf{Y}^r\mathbf{Y}^s} + \sigma_{rs}^2$$

$$r, s = \text{SW, TOT, LW.}$$

We have modeled I_λ as a random variable (or random function) over the ensemble of all possible scenes. Let us assume knowledge of a finite number (say N) of these possible scenes and approximate the expected value with a simple weighted average or

$$E[I_\lambda I_{\lambda'}] \approx \sum_{k=1}^{N} p^k I_\lambda^k I_{\lambda'}^k \equiv \overline{I_\lambda I_{\lambda'}},$$

where p^k is the probability of I_λ^k and $\Sigma_k\, \text{p}^k = 1$. We can formulate the spectral correction algorithm from (4) as

$$m^{\text{SW}}(D) = C_1 m_f^{\text{SW}}(D) + C_2 m_f^{\text{LW}}(D) + C_3 m_f^{\text{TOT}}(D)$$

$$m^{\text{LW}}(D) = C_4 m_f^{\text{SW}}(D) + C_5 m_f^{\text{LW}}(D) + C_6 m_f^{\text{TOT}}(D), \quad (5)$$

where C_i are the spectral correction coefficients (SCC), and D denotes daytime. Since we have the redundance of three filtered measurements to define two unfiltered measurements, we can use any two channels to determine the unfiltered measurements. If we unfilter with just the SW and TOT channels, then

$$m^{\text{SW}}(D) = C_7 m_f^{\text{SW}}(D) + C_8 m_f^{\text{TOT}}(D)$$

$$m^{\text{LW}}(D) = C_9 m_f^{\text{SW}}(D) + C_{10} m_f^{\text{TOT}}(D), \quad (6)$$

and if we unfilter with only the single channels, then

$$m^{\text{SW}}(D) = C_{11} m_f^{\text{SW}}(D)$$

$$m^{\text{LW}}(D) = C_{12} m_f^{\text{LW}}(D). \quad (7)$$

At night (denoted by N), the general expression is

$$m^{\text{LW}}(N) = C_{13} m_f^{\text{LW}}(N) + C_{14} m_f^{\text{TOT}}(N), \quad (8)$$

TABLE 2. Range of basic single-channel unfiltering coefficients (C_{11}, C_{12}, C_{16}).

Scene	Tropics $\lvert lat\rvert \leq 30°$	Midlatitude $30° < \lvert lat\rvert \leq 60°$	Polar $\lvert lat\rvert > 60°$
Ocean	1.7099–1.8152	1.6766–1.8079	1.6580–1.8310
	1.7591–1.7703	1.7873–1.8009	1.8211–1.8361
	1.1139–1.1144	1.1141–1.1148	1.1144–1.1151
Land	1.6799–1.8143	1.6633–1.7876	1.6725–1.7818
	1.7512–1.7613	1.7666–1.7853	1.8027–1.8179
	1.1139–1.1144	1.1141–1.1148	1.1145–1.1151
Snow		1.7226–1.8215	1.7157–1.8294
		1.8342–1.8448	1.8812–1.9193
		1.1144–1.1150	1.1156–1.1159
Desert	1.6923–1.8013		
	1.7362–1.7479		
	1.1138–1.1144		
Cloud	1.7126–1.7322	1.7064–1.7282	1.7044–1.7241
	1.8633–1.8692	1.8990–1.9000	1.8897–1.9091
	1.1145–1.1148	1.1155–1.1157	1.1154–1.1158

and for the single channels

$$m^{LW}(N) = C_{15} m_f^{LW}(N)$$
$$m^{LW}(N) = C_{16} m_f^{TOT}(N). \quad (9)$$

The SCC are mean values and thus introduce error into the process. This error was minimized by determining different coefficients for four basic cloudless scenes (ocean, land, desert, snow) and one cloudy scene. The basic coastal coefficients are the average of the ocean and land coefficients. The coefficients C_i for the 12 ERBE scenes in Table 1 were derived from these 6 basic scenes by linear interpolation on cloud amount, or for the ERBE production $C_i = (1 - \alpha)$(basic cloudless C_i) + α(cloudy C_i), where α is 0.025, 0.275, 0.725, and 0.975 for clear, partly cloudy, mostly cloudy, and overcast, respectively. The validity of linear interpolation will be discussed later.

In addition to variation with scene type, the coefficients also vary with latitude and viewing zenith, solar zenith, and relative azimuth angles due to the shift of the field spectral radiance with angle. Table 2 gives the range of the single-channel coefficients. For example, the coefficient that unfilters the shortwave radiance for clear ocean in the Tropics is C_{11}, which ranges from a minimum of 1.7099 to a maximum of 1.8152 depending on the solar zenith angle, the viewing zenith angle, and the viewing azimuth angle. This range corresponds to a 6.0% change in radiance. Over all scenes and latitude bands, the C_{11} range is 9.9%. The longwave unfiltering defined by C_{12} has a similar range of 10.0%. Thus, if we unfiltered with a single coefficient independent of scene type and viewing geometry, we would incur errors of ±5.0%. The spectral correction algorithm reduces these errors by modeling the scene spectral characteristics and by scene identification.

At night the single unfiltering of the TOT channel is accomplished with C_{16}, which has a range of 0.2% and is insensitive to the scene type. This insensitivity results from the flatness of the TOT channel over the 5–50-μm range (see Fig. 1).

Let us now concentrate on the Tropics. Table 3 defines the coefficients for a nadir viewing measurement at overhead sun. The general expression for determining $m^{SW}(D)$ involves C_1, C_2, and C_3 [see (5)]. From Table 3, we see that C_2 and C_3 are much smaller that C_1 so that the unfiltered shortwave measurement is derived almost entirely from the SW channel. Even in the extreme case where the SW channel radiance is small and the LW and TOT channel radiances are large, C_2 and C_3 will combine to approximately cancel the effect of the LW and TOT channels. By examining C_4, C_5, and C_6, we see that $m^{LW}(D)$ is basically the TOT channel minus the SW channel both weighted about equal. At night, C_{14} dominates so that $m^{LW}(N)$ is essentially derived from the TOT channel. Thus, the estimation equation (4) for the SCC recognize the LW channel response as being nonflat and more sensitive to scene variation than the other channels. Accordingly, the estimation process weights the LW channel effect very little. At night its relative effect is at most 2.2% and during the day 3.2%. However, the LW channel allows for redundancy and plays an important role when one channel is lost. The LW channel is crucial in the validation of all channels.

4. Comparison of longwave radiances at night

The longwave radiance at night can be determined from either the LW channel or the TOT channel. The TOT channel at night measures all the earth-emitted

TABLE 3. Spectral correction coefficients for the Tropics.

Coefficient	Ocean	Land	Desert	Cloud
Day				
C_1	1.7932	1.6572	1.6727	1.7365
C_2	0.0000	−0.0687	−0.0320	0.0076
C_3	−0.0014	0.0424	0.0193	−0.0064
C_4	−1.2586	−1.2511	−1.2514	−1.2911
C_5	0.0000	−0.0055	−0.0039	−0.0610
C_6	1.1149	1.1181	1.1172	1.1524
C_7	1.7932	1.7062	1.6957	1.7314
C_8	−0.0014	−0.0013	−0.0012	−0.0018
C_9	−1.2586	−1.2472	−1.2486	−1.2502
C_{10}	1.1149	1.1146	1.1146	1.1159
C_{11}	1.7844	1.7008	1.6923	1.7284
C_{12}	1.7591	1.7512	1.7362	1.8692
Night				
C_{13}	0.0097	−0.0003	−0.0026	−0.0418
C_{14}	1.1078	1.1141	1.1154	1.1397
C_{15}	1.7591	1.7637	1.7677	1.8513
C_{16}	1.1139	1.1139	1.1138	1.1145

energy from 0 to 200 μm (see Fig. 1), which is the proper quantity for determining the earth radiation budget. The LW channel measures the energy from 5 to 50 μm. The difference in spectral range between the two channels from 50 to 200 μm is resolved by the SCC. Recall that the unfiltered longwave measurement (3) is defined from 5 to 200 μm so that the regression (4) of the modeled filtered measurement (2) and the modeled unfiltered measurement (3) takes this range difference into account. The difference in range between 0 and 5 μm must be resolved. If we are to compare the longwave and total measurements for consistency, we must determine the emitted energy from 0 to 5 μm and subtract it from the total measurement.

We approximate the small amount of emitted energy from 0 to 5 μm as blackbody radiation to adjust the TOT channel. At night, we can determine the total flux from the TOT channel. We get the temperature from the Stefan–Boltzmann law. From the temperature and Planck's law, we get the blackbody radiation, which we integrate from 0 to 5 μm. Over all observed scenes and all viewing geometries, the amount of emitted energy from 0 to 5 μm varies from 0.01% to 0.37% of the total energy.

The comparison of the unfiltered longwave radiances in the Tropics at night from the LW channel and the adjusted TOT channel is given in Table 4. For all scenes, the mean flux at night was 256.53 W m^{-2} and the difference between the two channels was 0.95 W m^{-2} sr^{-1} with a standard deviation of 1.20 W m^{-2} sr^{-1}. Thus, the unfiltered longwave measurement is about 1.1% higher than the total measurement. This error is not equally distributed over the ERBE scene types. The four basic scene types for which SCC were developed (clear ocean, clear land, clear desert, overcast) have relatively small errors, while the partly cloudy scenes are about 1% in error and the mostly cloudy scenes are about 2% in error. This suggests that the linear interpolation of the SCC from clear to overcast is not justified for the LW channel.

Recall that our main purpose is to establish the stability and consistency of the unfiltered radiances at satellite altitude from which we determine the flux at the TOA. We take as our reference the TOT channel at night because of its spectral flatness and insensitivity to different scene types. We have seen that the LW channel measurement is about 1.1% high, but has little effect on the unfiltered radiances because of its low weighting. Thus, let us consider the ERBS production radiances as dependent only on the TOT and SW channels and use the LW channel to transfer our reference radiance from night to day. Moreover, let us revisit the unfiltering of the LW channel.

From Fig. 1, we see that the LW channel spectral response is not flat and monotonically decreasing with increasing wavelengths. This causes the SCC in Table 3 to vary widely from say clear ocean ($C_{15} = 1.7591$) to cloud ($C_{15} = 1.8513$). Table 4 shows that the linear interpolation for partly cloudy and mostly cloudy scenes is not justified. Thus, let us determine a new set of SCC for the LW channel by matching the LW channel to the TOT channel since the TOT channel is insensitive to scene type. Moreover, let us determine both a multiple A_i and an offset B_i as

TABLE 4. Three-channel intercomparison of longwave radiance in the Tropics for ERBS on 13 April 1985.

	Daytime $\Delta m^{LW}(D) = \left(C_{10}m_f^{TOT} + C_9 m_f^{SW}\right) - C_{12}m_f^{LW}$					Nighttime $\Delta m^{LW}(N) = C_{15}m_f^{LW} - C_{16}m_f^{TOT}$				
Scene	Mean flux F^{LW} (W m^{-2})	Std Dev flux F^{LW} (W m^{-2})	Number of samples	Mean Δm^{LW} (W m^{-2} sr^{-1})	Std Dev Δm^{LW} (W m^{-2} sr^{-1})	Mean flux F^{LW} (W m^{-2})	Std Dev flux F^{LW} (W m^{-2})	Number of samples	Mean Δm^{LW} (W m^{-2} sr^{-1})	Std Dev Δm^{LW} (W m^{-2} sr^{-1})
Clear										
Ocean	297.10	8.35	924	0.49	0.62	298.84	6.55	387	0.13	0.43
Land	334.15	25.30	111	−0.81	1.16	283.14	11.85	36	−0.18	0.54
Desert	331.36	18.87	238	0.24	0.82	280.14	12.31	237	−0.42	0.51
Coastal	303.49	21.19	28	0.06	0.73	300.35	8.39	31	−0.71	0.39
Partly cloudy										
Ocean	280.10	9.47	1367	−0.96	0.71	279.60	8.34	1605	1.15	0.64
Land	285.65	21.25	283	−1.01	0.97	260.22	20.60	242	0.86	0.73
Coastal	277.51	17.29	61	−1.27	0.86	270.72	12.70	76	0.95	0.58
Mostly cloudy										
Ocean	245.52	20.49	663	−2.33	1.03	245.69	15.39	732	2.34	0.91
Land	239.38	23.68	160	−1.81	1.17	219.69	13.40	189	1.14	0.98
Coastal	237.52	18.25	58	−2.03	1.09	236.73	13.14	23	1.87	0.91
Overcast	164.86	35.46	512	−0.33	1.32	162.74	39.89	511	−0.30	1.34
All scenes	267.63	47.77	4405	−0.77	1.29	256.53	44.17	4069	0.95	1.20

$$m^{LW} = A_i m_f^{LW} + B_i. \quad (10)$$

The unfiltering of the LW channel with only a multiple (9) assumes that the filtered radiance is always a constant percent of the radiance independent of the variation within the scene. However, we know the energy spectrum shifts to higher wavelengths for colder scenes, and, due to the monotonic decrease of the longwave spectral response, the LW channel measures a smaller percent for cold scenes and a larger percent for hot scenes. Thus, we need both a multiple and offset in (10) to model the longwave radiance accurately. The need for a longwave offset becomes clear by examining a scatter diagram of the measured total radiances versus the measured longwave radiances.

A new set of SCC for each scene type was determined by matching the LW and TOT channel radiances at night for 4 months spaced over the ERBS 5-yr scanner lifetime. The SCC were determined by linearly regressing the adjusted unfiltered TOT channel radiances at night on the corresponding filtered LW channel radiances at night for all measurements of the same scene type over the 4-month dataset. Coefficients A_i and B_i (10) were determined so that the adjusted unfiltered TOT channel and the unfiltered LW channel radiances were matched in a least squared sense. In addition, an SCC independent of scene was determined as

$$m^{LW}(N) = 1.6463 m_f^{LW}(N) + 6.3200, \quad (11)$$

which is similar to the individual scene SCC. Note the large offset of 6.32 W m^{-2} sr^{-1}. Results for one day are given in Table 5 for these new SCC. These results are typical of other days. First, we see that the longwave channel is matched to the TOT channel at night and for 13 April 1985, was only 0.10 W m^{-2} sr^{-1} different. Most significant is the reduction in the standard deviation of this difference from 1.20 W m^{-2} sr^{-1} for the ERBS production SCC to 0.54 W m^{-2} sr^{-1} for the new SCC. Using only one SCC for all scenes, as in (11), only increases the standard deviation from 0.54 to 0.59 W m^{-2} sr^{-1}. Thus, we see that the new SCC are much more accurate and less sensitive to scene types, which gives validity to the inclusion of a constant offset term in the SCC model (10). Also, we see that the increase in $\Delta m^{LW}(N)$ from clear to partly cloudy and mostly cloudy for the production SCC has been removed.

5. The shortwave channel at night

The ERBS shortwave measurement at night was very erratic and difficult to model. During a single day, the satellite experienced about 15 nighttime passages or one every orbit. The average nighttime passage shortwave measurement generally varied from −0.2 to +0.5 W m^{-2} sr^{-1}. These measurements represent a significant deviation from zero since the average daytime shortwave measurement on a terminator orbit (6 April 1985) is 21 W m^{-2} sr^{-1}, and for clear ocean the average shortwave measurement is only 8 W m^{-2} sr^{-1}. On a noon orbit (20 April 1985) the daytime shortwave measurements are about twice the terminator orbit values. Thus, nighttime measurements can easily represent from 1% to 2% of the daytime measurements. Two

TABLE 5. Three-channel intercomparison of longwave radiance in the Tropics for ERBS on 13 April 1985, for new longwave coefficients.

	Daytime $\Delta m^{LW}(D) = \left(C_{10} m_f^{TOT} + C_9 m_f^{SW}\right) - \left(A_i m_f^{LW} + B_i\right)$					Nighttime $\Delta m^{LW}(N) = \left(A_i m_f^{LW} + B_i\right) - C_{16} m_f^{TOT}$				
Scene	Mean flux F^{LW} (W m^{-2})	Std Dev flux F^{LW} (W m^{-2})	Number of samples	Mean Δm^{LW} (W m^{-2} sr^{-1})	Std Dev Δm^{LW} (W m^{-2} sr^{-1})	Mean flux F^{LW} (W m^{-2})	Std Dev flux F^{LW} (W m^{-2})	Number of samples	Mean Δm^{LW} (W m^{-2} sr^{-1})	Std Dev Δm^{LW} (W m^{-2} sr^{-1})
Clear										
Ocean	297.10	8.35	924	0.34	0.63	298.84	6.55	387	0.23	0.42
Land	334.15	25.30	111	−0.50	0.77	283.14	11.85	36	0.09	0.47
Desert	331.36	18.87	238	0.23	0.68	280.14	12.31	237	−0.30	0.60
Coastal	303.49	21.19	28	−0.10	0.66	300.35	8.39	31	−0.69	0.43
Partly cloudy										
Ocean	280.10	9.47	1367	0.33	0.70	279.60	8.34	1605	0.12	0.52
Land	285.65	21.25	283	0.29	0.61	260.22	20.60	242	0.18	0.64
Coastal	277.51	17.29	61	−0.10	0.55	270.72	12.70	76	0.03	0.59
Mostly cloudy										
Ocean	245.52	20.49	663	0.40	0.67	245.69	15.39	732	0.13	0.51
Land	239.38	23.68	160	0.72	0.87	219.69	13.40	189	0.03	0.46
Coastal	237.52	18.25	58	0.30	0.86	236.73	13.14	23	0.04	0.43
Overcast	164.86	35.46	512	−0.15	0.73	162.74	39.89	511	0.12	0.57
All scenes	267.63	47.77	4405	0.26	0.72	256.53	44.17	4069	0.10	0.54

consecutive nighttime passages can have average shortwave measurements that differ by as much as 0.3 W m^{-2} sr^{-1}. The shortwave measurement can jump by as much as 0.3 W m^{-2} sr^{-1} at internal calibration events. For these reasons, the ERBE processing system set the SW channel to zero at night. During an orbital nighttime passage, the average shortwave measurement was determined and subtracted from the shortwave measurement on the following daytime passage.

Although there is no reflected shortwave energy at night, the SW channel will detect thermal energy in the 0.2–5-μm range just as the TOT channel did. Over all observed scenes, this blackbody radiance has a mean of 0.07 W m^{-2} sr^{-1} and a standard deviation of 0.03 W m^{-2} sr^{-1}. The ERBE production algorithms set the SW channel to zero at night instead of a small positive amount. This oversight causes the daytime shortwave to be 0.07 W m^{-2} sr^{-1} low.

We see from Fig. 1 that the SW channel will also detect a small amount of energy from 60 to 200 μm. Over all observed scenes, this amount has a mean of 0.08 W m^{-2} sr^{-1} and a standard deviation of 0.005 W m^{-2} sr^{-1}. By setting the shortwave measurement to zero at night, the ERBE processing algorithms correct this problem.

6. Comparison of longwave radiances for daytime

We have seen that the effect of the LW channel on the ERBE production processing is negligible so that we can consider the ERBE processing as using only the SW and TOT channels as in (6). Thus, the production longwave radiance during the daytime is effectively derived from the TOT channel radiance minus the SW channel radiance with the appropriate weighting. We can also derive the longwave radiance from the LW channel radiance by (7). Table 4 gives the difference between these two estimates of daytime longwave radiance for the ERBS production SCC. For all scenes, this difference is −0.77 W m^{-2} sr^{-1}. Again, as with the nighttime differences, we see the four basic spectral correction scenes with small differences, while the partly cloudy scenes are about 1% inconsistent and the mostly cloudy scenes are about 2% inconsistent. We attribute these differences to the inadequate linear assumption of SCC with cloud amount for the longwave channel and the lack of a constant offset term. Next, consider the daytime differences based on the new coefficients (10) as given in Table 5, which show very good results with seemingly random differences over the scene types. For all scenes, this difference was reduced from −0.77 to 0.26 W m^{-2} sr^{-1}, and the standard deviation was reduced from 1.29 to 0.72 W m^{-2} sr^{-1}. We conclude from the data in Table 5 that the daytime longwave radiance is high by 0.3% relative to the LW channel radiance, which is matched to the reference TOT channel at night.

We now want to determine the consistency of the daytime shortwave radiances. Comparing the shortwave radiances directly is difficult because of the large variation and because it is not clear how to adjust the shortwave and total SCC for nonlinearity during the daytime. It is much easier to examine the longwave difference and infer the shortwave inconsistency. For the sake of discussion, let us assume the daytime longwave difference is $+\Delta m^{LW}(D)$. Since the longwave radiances from the LW channel and TOT channel are matched, we see from the $\Delta m^{LW}(D)$ equation in Table 5 that this difference must be the result of the SW channel measuring low (C_9 is negative) or the shortwave part of the TOT channel measuring high, or a combination of the two sources of error. Recall from (5) and Table 3 that the shortwave radiance is almost entirely based on the SW channel. Thus, it is important to determine the source of the longwave difference since an error in the shortwave part of the TOT channel does not affect the daytime shortwave radiance, while an error in the SW channel directly affects the daytime shortwave radiance. We will examine which shortwave source is causing the longwave inconsistency in a later section, where we have a 5-yr data history to examine.

7. Monthly variation of comparisons

We have examined the three-channel intercomparison for 13 April 1985 in Table 5. Now let us examine the entire month of April 1985. Figure 2 presents the nighttime and daytime longwave difference for each day during the month for all scenes. Also shown is the average shortwave measurement for each day. The increase and decrease of the shortwave measurement results from the ERBS orbit that has an inclination of 57° with a precessing node of about −5° per day. At the beginning of the month the orbit is in a late afternoon orbit and precesses to a noon orbit on 20 April and then to a morning orbit at the end of the month. During the first part of the month, the terminator orbit results in very poor sampling conditions. Days 1 and 2 have no

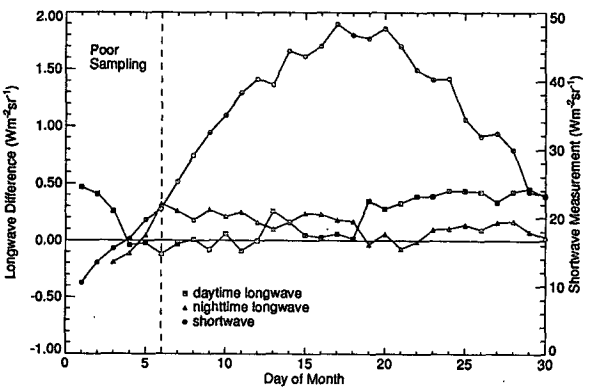

FIG. 2. Daily mean longwave difference Δm^{LW} for April 1985 for all scenes. Also shown is the daily mean filtered shortwave measurement $\bar{m}_f^{SW}(D)$.

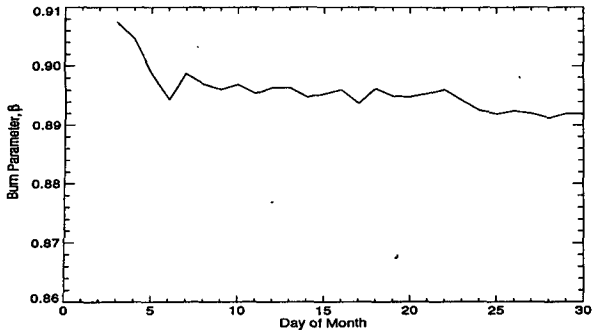

FIG. 3. Daily burn parameter β for overcast scenes for April 1985.

nighttime measurements such that the solar zenith was greater than 114°. For the purpose of our validation, we will define the useful time period to be from 6 April to 30 April.

From Fig. 2, we see that the nighttime longwave comparison is reasonably constant and varies very little from day to day. Its full range from 6 April to 30 April is -0.07 to 0.32 W m^{-2} sr^{-1} for an average of 0.14 W m^{-2} sr^{-1}. The daytime longwave comparison is at its minimum of -0.12 W m^{-2} sr^{-1} at the beginning of the month and gradually increases reaching its maximum of 0.46 W m^{-2} sr^{-1} near the end of the month for an average of 0.20 W m^{-2} sr^{-1}. From this figure, we conclude that the longwave comparison is independent of the solar orientation except during the extreme terminator conditions. Thus, for the 5-yr lifetime of the scanner, we will determine a monthly longwave comparison by averaging 3 or 4 days separated by 1 week.

Another parameter that remains relatively constant over various geometries and is useful for validation is presented in Fig. 3. We refer to it as the "burn parameter," which will become obvious presently. Its form is given by

$$\beta = \frac{\bar{m}_f^{\mathrm{SW}}(D) - \bar{m}_f^{\mathrm{SW}}(N)}{\bar{m}_f^{\mathrm{TOT}}(D) - \bar{m}_f^{\mathrm{TOT}}(N) - \dfrac{1.66}{1.12}\left[\bar{m}_f^{\mathrm{LW}}(D) - \bar{m}_f^{\mathrm{LW}}(N)\right]}, \quad (12)$$

where the bar denotes daily average. The parameter β is best explained as an estimate of the ratio of the filtered radiance from the SW channel to the filtered radiance from the shortwave part of the TOT channel. Moreover, the radiance is the difference between daytime radiance and nighttime radiance over overcast areas in the Tropics ($\pm 30°$ latitude). Subtracting the nighttime radiance from the daytime radiance eliminates any constant additive offset error. The difference in radiance from the SW channel is the average daytime filtered shortwave measurement $\bar{m}_f^{\mathrm{SW}}(D)$ minus the average uncorrected nighttime measurement. The denominator is the average daytime filtered total measurement, $\bar{m}_f^{\mathrm{TOT}}(D)$, minus an estimate of the longwave measurement on the TOT channel. We have chosen overcast scenes to minimize the diurnal change from night to day. Thus, $\bar{m}_f^{\mathrm{TOT}}(N)$ is the nighttime measurement but should be similar to the daytime longwave part of the measurement. A small diurnal and sampling correction is made by differencing the LW channel for day and night and adjusting it with the single channel SCC so that it is compatible with the TOT channel.

The burn parameter has several interesting characteristics. Any scene type can be used to define β. A good choice is all ocean scenes that require no scene identification other than to distinguish between land and ocean. This eliminates all discussion of scene identification errors. Another choice is all overcast scenes that require a scene identification algorithm. We have found that overcast scenes with their larger component of shortwave radiance proved to yield the most constant β over various sun geometries. The burn parameter is also independent of the spectral correction process working only with filtered data. The only exception is the ratio of SCC. The LW channel measurement for overcast is approximately unfiltered with 1.66 from (10) and approximately filtered to match the TOT channel by 1.12 from C_{10} in Table 3. This ratio is held constant for all overcast scenes. The β involves all three channels so that any inconsistency is identified. Figure 3 presents the burn parameter for the month of April 1985. Except for the first part of the month, it is remarkably constant and shows no effect of the precessing orbit and the changing sun condition. We will use this parameter in the validation of the scanner channels.

8. Yearly variation of comparisons

A time history of the longwave comparisons for the lifetime of the ERBS scanner is given in Fig. 4. The ERBS was launched October 1984, and the first full month of data is for November 1984. The scanner continued for 64 months and failed on 28 February 1990. The longwave difference at night seems to be relatively small and constant at least after June 1986. However,

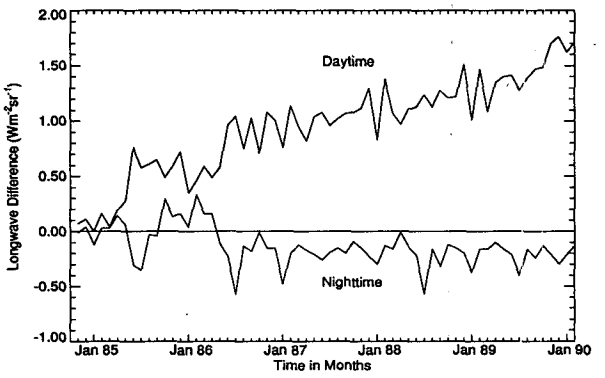

FIG. 4. Time history of longwave difference for each month of ERBS scanners.

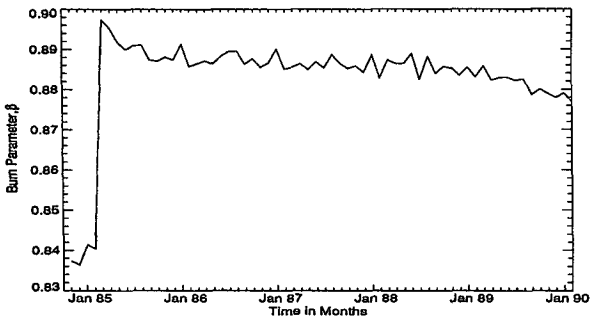

FIG. 5. Time history of burn parameter β for each month of ERBS scanners.

the daytime longwave comparison shows a dramatic increase over the 64-month period. Since the TOT and LW channels agree at night, the daytime increase represents a shortwave error. This is also confirmed by Fig. 5, which shows a gradual drop in the burn parameter over the period. It will take additional analysis to determine which of the channels is changing with time.

Figure 5 shows a dramatic jump in the burn parameter between February and March 1985 from about 0.84 to 0.89. This resulted from inadvertently scanning the sun and damaging the shortwave part of the TOT channel. On 20 February, the ERBS satellite was in full or near-full sun and the scanners were stowed. On 25 February, the scanners were commanded to return to a normal cross-track scan. However, the scanner azimuth beam did not return to its normal position of 180°, but remained at its calibration position of 35.9°. The azimuth position indicator used a light source to sense the position, and the design permitted exposure to external light, which caused the output counter to reset causing the mislocation. A full discussion is given by Weaver et al. (1991). On 28 February, the scanner viewed the sun directly and the shortwave part of the TOT channel output was reduced by about 6.5%, causing the increase in β. A possible mechanism for the observed change is the TOT channel active flake deteriorated upon being exposed to rather well-focused ultraviolet solar radiation. The SW channel filter and window apparently shielded that channel's flake surface sufficiently to prevent its damage, and the LW channel flake was exposed only to solar infrared. One of the main parameters to show the change was the "burn parameter" (12) from which it gets its name. This change was modeled as a uniform decrease of 6.5% in the spectral response of the shortwave part of the TOT channel S_λ^{TOT}. A new set of SCC was generated with this new spectral response and successfully used on all ERBS scanner data after 1 March 1985.

The ERBS orbit was designed to approximately repeat monthly and yearly so that 10 April 1989 has almost the same orbital geometry as 13 April 1985, 4 years earlier. The 3-day shift was necessary to get the best match in sampling geometry. The latitude of the sun changed little over these 3 days. A comparison of 10 April and 13 April clearly shows the daytime longwave difference has increased over the 4 years from 0.26 W m^{-2} sr^{-1} in Table 5 to 1.46 W m^{-2} sr^{-1}, while the nighttime difference remained small. We must examine the three channels to determine the source of change.

We can form significant statistical tests of changes in the three channels by differencing the daily averages over the month of April. Figure 6 shows the repeatability of the daily mean shortwave $\bar{m}_f^{\mathrm{SW}}(D)$ for April 1985 and 1989, where the April 1989 data have been shifted by 3 days. Due to the extreme geometry on the terminator orbit at the beginning of the month, we compare only the 25 days of 6–30 April 1985 with 3–27 April 1989. Thus, we have 25 independent measurements of the daily change in the SW channel. The mean change is -0.22 W m^{-2} sr^{-1} and the standard deviation is 2.29. The standard deviation of the mean is smaller by the square root of 25 or 0.46 W m^{-2} sr^{-1}.

We can test the hypothesis that the mean change is zero by dividing the mean by its standard deviation and forming the test statistic Z. If Z is greater than 1.96, then we conclude at the 5% significance level that the mean difference is not zero, but has changed. An estimate of the change is the mean itself. The statistical tests on all channels are given in Table 6 for clear ocean scenes that have smaller standard deviations than all scenes and give stronger tests. Using the data for all scenes, we could not conclude a change in any of the three channels. However, it was clear that the longwave difference Δm^{LW} had changed for both day and night. We see from Table 6 that the TOT channel at night is remarkably constant. This was also true for all scenes and was confirmed on other months. Since the Z statistic is -0.13 and since the absolute value does not exceed 1.96, we cannot conclude a change with certainty. Thus, we will consider the TOT channel at night as unchanged. We also see that the LW channel has a significant change. At night, we estimate the change at

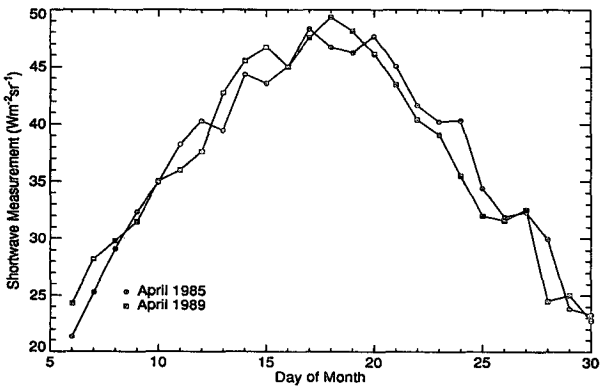

FIG. 6. Comparison of daily mean filtered shortwave measurement $\bar{m}_f^{\mathrm{SW}}(D)$ for April 1985 and April 1989.

TABLE 6. Hypothesis test for change in radiance measurements from April 1985 to April 1989 for clear ocean scenes.

	Daytime				Nighttime			
	m_f^{SW}	m_f^{LW}	m_f^{TOT}	$\Delta m^{LW}(D)$	m_f^{SW}	m_f^{LW}	m_f^{TOT}	$\Delta m^{LW}(N)$
Mean of daily means for Apr 85 (W m^{-2} sr^{-1})	12.86	55.27	102.23	0.23	0.04	56.06	88.91	0.16
Mean of daily means for Apr 89 (W m^{-2} sr^{-1})	13.11	54.95	102.86	1.14	−0.20	55.87	88.90	−0.14
Std of daily means for Apr 85 (W m^{-2} sr^{-1})	3.17	0.32	3.75	0.18	0.07	0.28	0.40	0.14
Std of daily means for Apr 89 (W m^{-2} sr^{-1})	3.53	0.29	4.40	0.19	0.07	0.29	0.44	0.09
Mean of daily difference for Apr 89 minus Apr 85 (W m^{-2} sr^{-1})	0.25	−0.32	0.63	0.91	−0.24	−0.19	−0.01	−0.30
Std of daily difference for Apr 89 minus Apr 85 (W m^{-2} sr^{-1})	0.73	0.30	0.97	0.19	0.10	0.33	0.50	0.13
Test statistic Z	1.71	−5.43	3.27	23.97	−11.71	−2.89	−0.13	−11.26

−0.19 W m^{-2} sr^{-1} and during the day at −0.32 W m^{-2} sr^{-1}. Since these two estimates are not statistically different, we combine the two and estimate a LW channel filtered radiance decrease of −0.25 W m^{-2} sr^{-1}, which by (11) will change Δm^{LW} by approximately −0.41 W m^{-2} sr^{-1}. Half of this change seems to be a positive bias on April 1985 and the other half a negative bias on April 1989. From examining Fig. 4 we see that the longwave differences at night behave erraticly until June 1986 when they stabilize. From November 1984 to May 1986 the nighttime differences average to 0.03 W m^{-2} sr^{-1}. From June 1986 to February 1990 they average −0.21 W m^{-2} sr^{-1}. This would imply that the unfiltered radiance from the LW channel has changed by less than the −0.41 W m^{-2} sr^{-1} from the hypothesis test. It is not clear why these two estimates disagree, nevertheless, the change in the LW channel is small, being less than 0.5% in 4 years, and does not further effect the TOA fluxes.

The change in the LW channel is important only so that we do not attribute this change to the shortwave during the day. During the daytime, we see a significant $\Delta m^{LW}(D)$ change of 0.91 W m^{-2} sr^{-1}. We attribute 0.41 W m^{-2} sr^{-1} to a change in the LW channel so that 0.50 W m^{-2} sr^{-1} must be attributed to a shortwave change. The SW channel has a Z of 1.71, so we assume no change in the SW channel. However, the TOT channel shows a significant change over the 4 years with a Z of 3.27. Since the TOT channel shows a change during the day and no change at night, we conclude the shortwave part of the TOT channel has changed so that $\Delta m^{LW}(D)$ changes by 0.50 W m^{-2} sr^{-1}. Thus, we con-

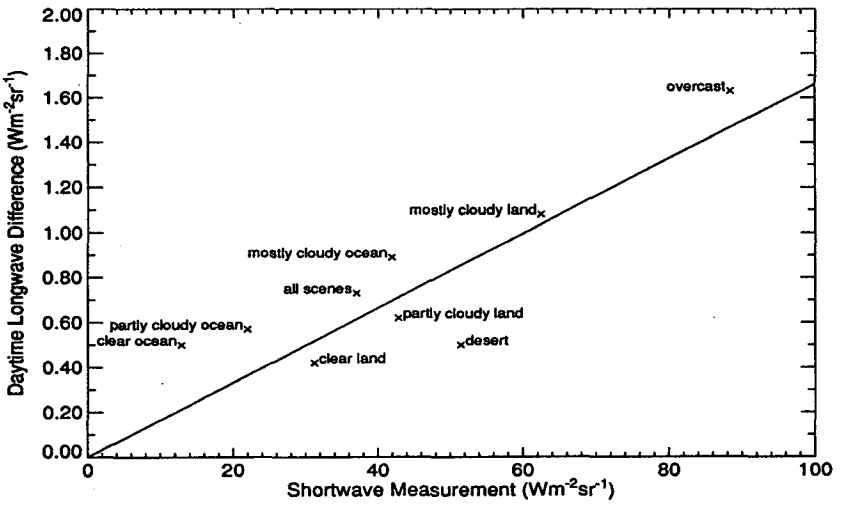

FIG. 7. Comparison of the daytime longwave difference with the mean shortwave measurement. The daytime longwave difference is the change in the longwave difference from April 1985 to April 1989, corrected for a 0.41 W m^{-2} sr^{-1} decrease in the longwave channel. The shortwave measurement is the monthly mean filtered shortwave measurement for April 1985. The regression line shows an increase in the longwave difference with the magnitude of the shortwave measurement.

clude the longwave comparison growth during the day is entirely from a change in the shortwave part of the TOT channel.

We can determine whether the change is a gain or constant offset by plotting the average shortwave measurement versus the change in $\Delta m^{LW}(D)$ for different scene types. Figure 7 shows that the 4-yr $\Delta m^{LW}(D)$ increases versus the mean of the daily shortwave for April 1985. A regression fit to the data gives a slope of 0.0147 and an intercept of 0.13 W m^{-2} sr^{-1}, which is not statistically different than zero. Accordingly, we assume the intercept is zero and determine a slope of 0.0166, which represents an increase in the gain of the shortwave part of the TOT channel of 1.3% over 4 years.

Another approach to determining the gain change in the shortwave part of the TOT channel is with the burn parameter. We determined 25 daily β's for 6–30 April 1985. The mean of the daily β's was 0.8964 with a standard deviation of 0.0020. The corresponding values for 3–27 April 1989 were 0.8827 and 0.0021. Ratioing the two β's gives the desired gain change of 1.013. A Monte Carlo analysis further gives the standard deviation of the gain increase as 0.1%. Thus, once we know the source of the change, the burn parameter is an expedient way to obtain the magnitude and variance of the change. The longwave comparison (Fig. 4) suggests the change is linear in time. However, from the β history (Fig. 5), it is clear that the change is not linear but varies with time. The shortwave part of the TOT channel seems to increase for about a year after the sun damage of February 1985, and then stabilizes until the last year when it dramatically increases and reduces β. The cause of this nonlinear change is not clear.

We can now summarize how all these changes affect the ERBS fluxes at the TOA. First, the longwave radiance at night is derived almost entirely from the TOT channel, which we have taken as our reference. We have observed no change in the TOT channel over the 4-yr period. Thus, we know of no measurement inconsistencies in the nighttime longwave flux. The daytime longwave comparison shows a shortwave gain problem that we attribute to the shortwave part of the TOT channel. The SW channel shows no statistically significant change over the 4 years so that we know of no measurement inconsistencies in the daytime shortwave flux, which is derived from the SW channel. The daytime longwave flux, however, is effected by a 1.3% gain change in the shortwave part of the TOT channel over the 4 years. This only effects the daytime longwave flux, depending on its shortwave component. Table 7 gives the average TOA flux error for April 1989. The effect on clear ocean is small (0.63 W m^{-2} or 0.2%) because its shortwave component is small. For bright overcast scenes, the shortwave dominates so that the longwave bias is large (4.34 W m^{-2} or 2.6%). On average for all scenes, the longwave bias is less than 1%.

TABLE 7. Mean error in daytime longwave flux at the TOA in the Tropics for ERBS in April 1989.

Scene	Daytime longwave flux mean error (W m^{-2})	(%)
Clear		
Ocean	0.63	0.2
Land	1.53	0.5
Desert	2.52	0.7
Coastal	1.02	0.3
Partly cloudy		
Ocean	1.07	0.4
Land	2.10	0.7
Coastal	1.62	0.6
Mostly cloudy		
Ocean	2.06	0.8
Land	3.06	1.3
Coastal	2.68	1.1
Overcast	4.34	2.6
All scenes	1.81	0.7

9. Summary

More than 5 years of ERBS scanner radiance data have been processed to fluxes at the top of the atmosphere. The redundancy between the shortwave, longwave, and total scanning radiometers and data averages have been used to validate the long-term consistency among the measurements and to establish how measurement drift has affected the archived fluxes. Since the spectral response of the longwave channel is nonflat, the data processing relied almost entirely on the other two channels. Basically, the daytime shortwave flux is derived from the shortwave channel and the daytime longwave flux is derived from the total channel minus the shortwave channel. The nighttime longwave flux is derived from the total channel. The longwave part of the total channel has a flat spectral response and is therefore insensitive to the viewed scene and the scene identification errors. It also has shown remarkable stability over the years. For these reasons the total channel at night was taken as a reference and the other channels were compared to it. The longwave channel was matched to the total channel with new spectral correction coefficients so that the longwave reference could be transferred from night to day. The longwave flux from the total and shortwave channels was then validated against the longwave reference.

The longwave difference for daytime over a 4-yr test period changed from 0.26 to 1.46 W m^{-2} sr^{-1}. Hypothesis tests on monthly data averages showed that the shortwave part of the total channel was the culprit, and a regression on various scene types with varying shortwave components showed that the error was a gain increase of 1.3% over 4 years. Examination of the β

time history shows that the change is not linear but varies with time.

The objective of this study was to determine the change in the top of the atmosphere flux due to drift in the scanner measurements. Scene identifications and angular distributions model errors have not been considered. The flux at night is from the total channel that shows no evidence of change over the 4 years. Relative to the total channel at night, the daytime shortwave flux shows no change. The daytime longwave flux, however, is affected by the gain change over time which depends on the scene shortwave component. For clear ocean scenes with small shortwave component, the increase was 0.2% and for overcast scene the increase was 2.6%. For all scenes, the daytime longwave flux increased by less than 1% over 4 years.

The results of this study are in agreement with the results from the onboard calibration systems (Lee et al. 1991, 1992, 1993). Barkstrom et al. (1990) stated that there is no evidence from the onboard calibration systems for systematic effects greater than 0.5%. This is true because the one problem area for ERBS, the shortwave part of the total channel, was only monitored from November 1984 to October 1985 by the onboard calibration systems. This study has strengthened the validity of ERBS scanner data and defined the precision of the instruments to tenths of a percent, which the onboard calibration systems were not able to do.

REFERENCES

Bandeen, W. R., 1982: Earth radiation science seminars. NASA Conf. Publication 2239, US Government Printing Office, Washington, D.C., 1–28.

——, M. Halev, and I. Strange, 1965: A radiation climatology in the visible and infrared from the Tiros meteorological satellites. NASA Tech. Note TN D-2534, 30 pp.

Barkstrom, B. R., 1984: The Earth Radiation Budget Experiment (ERBE). *Bull. Amer. Meteor. Soc.,* **65,** 1170–1185.

——, and G. L. Smith, 1986: The Earth Radiation Budget Experiment: Science and implementation. *Rev. Geophys.,* **24,** 379–390.

——, E. F. Harrison, and R. B. Lee III, 1990: Earth Radiation Budget Experiment: Preliminary seasonal results. *Eos, Trans. Amer. Geophys. Union,* **71,** 297–305.

House, F. B., A. Gruber, G. E. Hunt, and A. T. Mecherikunnel, 1986: History of satellite missions and measurements of the earth radiation budget (1957–1984). *Rev. Geophys.,* **24,** 357–377.

Kopia, L. P., 1986: Earth Radiation Budget Experiment scanner instrument. *Rev. Geophys.,* **24,** 400–406.

Lee, R. B., III, and B. R. Barkstrom, 1991: Characterization of the Earth Radiation Budget Experiment radiometers. *Metrologia,* **28,** 183–187.

——, ——, N. Halyo, M. A. Gibson, and L. M. Avis, 1989: Characterizations of the Earth Radiation Budget Experiment (ERBE) scanning radiometers. *Proc. SPIE,* **1109,** 186–194.

——, L. M. Avis, M. A. Gibson, and L. P. Kopia, 1992: Characterizations of the mirror attenuator mosaic: Solar diffuser plate. *Appl. Opt.,* **31,** 6643–6652.

——, ——, ——, S. Thomas, and R. Wilson, 1993: In-flight evaluations of tungsten calibration lamps using shortwave thermistor bolometers and active-cavity radiometers. *Metrologia,* **30,** 389–395.

Liebelt, P. B., 1967: *An Introduction to Optimal Estimation.* Addison-Wesley, 273 pp.

Smith, G. L., R. N. Green, E. Raschke, L. M. Avis, J. T. Suttles, B. A. Wielicki, and R. Davies, 1986: Inversion methods for satellite studies of the earth's radiation budget: Development of algorithms for the ERBE mission. *Rev. Geophys.,* **24,** 407–421.

Suttles, J. T., R. N. Green, P. Minnis, G. L. Smith, W. F. Staylor, B. A. Wielicki, I. J. Walker, D. F. Young, V. R. Taylor, and L. L. Stowe, 1988: Angular radiation models for earth–atmosphere system, vol. 1, Shortwave radiation. NASA Ref. Publ. RP-1184, 144 pp.

——, ——, G. L. Smith, B. A. Wielicki, I. J. Walker, V. R. Taylor, and L. L. Stowe, 1989: Angular radiation models for the earth–atmosphere system, vol. 2, Longwave radiation. NASA Ref. Publ. RP-1184, 84 pp.

Weaver, W. L., K. A. Bush, C. J. Harris, C. E. Howerton, and C. J. Tolson, 1991: Mission description and in-flight operations of ERBE instruments on ERBS and NOAA 9 spacecraft: November 1984 through January 1986. NASA Ref. Publ. RP-1256, 281 pp.

Wielicki, B. A., and R. N. Green, 1989: Cloud identification for ERBE radiation flux retrieval. *J. Appl. Meteor.,* **28,** 1133–1146.